

# A cleaner processing approach for cellulose reinforced thermoplastic polyurethane nanocomposites

Khairatun Najwa Mohd Amin<sup>1,2</sup>  | Celine Chaleat<sup>1,3</sup>  | Grant Edwards<sup>1,4</sup>  |  
Darren J. Martin<sup>1,3</sup>  | Pratheep Kumar Annamalai<sup>1</sup> 

<sup>1</sup>Australian Institute for Bioengineering and Nanotechnology (AIBN), The University of Queensland, Brisbane, Queensland, Australia

<sup>2</sup>Faculty of Chemical and Process Engineering Technology, College of Engineering Technology, Universiti Malaysia Pahang, Gambang Kuantan, Pahang D.M., Malaysia

<sup>3</sup>School of Chemical Engineering, The University of Queensland, Brisbane, Queensland, Australia

<sup>4</sup>School of Mechanical and Mining Engineering, The University of Queensland, Brisbane, Queensland, Australia

## Correspondence

Khairatun Najwa Mohd Amin, Faculty of Chemical and Process Engineering Technology, College of Engineering Technology, Universiti Malaysia Pahang, Gambang Kuantan, Pahang D.M., 26300, Malaysia.

Email: knajwa@ump.edu.my

Pratheep Kumar Annamalai, Australian Institute for Bioengineering and Nanotechnology (AIBN), The University of Queensland, Brisbane, Queensland, 4072, Australia.

Email: p.annamalai@uq.edu.au

## Abstract

In a manner of addressing challenges in scalable processing of thermoplastic polyurethane (TPU) nanocomposites through extrusion methods, this study reports a very clean processing approach of incorporating cellulose nanocrystal (CNC) into a TPU matrix, with no acid or organic-solvents usage. It involves a mechanical deconstruction of microcrystalline cellulose (MCC) into nanoscale particles in water and polyol through scalable bead-milling, vacuum drying, and followed by twin-screw reactive extrusion with isocyanate and chain extender. The thermal stability of CNC was higher than that of typically acid-hydrolyzed CNC and suitable for processing with the precursors of TPU at typical processing temperature range (175–190°C). The CNC incorporation at very low loadings (0.5, 0.8 wt%) through this methodology resulted in substantial enhancements in tensile properties (for example, up to 28% in strength and toughness) without any significant stiffening effect. Moreover, the nanocomposites retained elastic properties, including elongation at break (%), resilience, and creep resistance. Their chemical properties and thermal transitions were also found to support the retained thermoplastic behavior while improving mechanical performance.

## KEYWORDS

cellulose nanocrystal (CNC), microcrystalline cellulose (MCC), nanocomposites, reactive extrusion, thermoplastic polyurethane

## 1 | INTRODUCTION

The improvement or modification of polymer properties using a wide range of nanoscale particles has been explored for last four decades.<sup>[1]</sup> In the field of polymer nanocomposites, the most suitable processing route relies on the thermal and physico-chemical

properties of the chosen nanofiller(s) and host polymer along with a target property profile of the final product.<sup>[2]</sup> The shift from laboratory to extensive application of polymer nanocomposites can only be accomplished by an industrially scalable process that delivers a favorable cost–performance ratio with low environmental impact.<sup>[3,4]</sup> The nanocellulose, which

This is an open access article under the terms of the Creative Commons Attribution-NonCommercial License, which permits use, distribution and reproduction in any medium, provided the original work is properly cited and is not used for commercial purposes.

© 2022 The Authors. *Polymer Engineering & Science* published by Wiley Periodicals LLC on behalf of Society of Plastics Engineers.

can be typically derived from plant biomass and some marine animals, is now being explored as sustainable and safe nanofiller for a new class of polymer nanocomposites.<sup>[5]</sup> While being renewable, environmentally benign, and low cost, the cellulose nanocrystal (CNC) exhibits very high specific mechanical properties (strength and stiffness).<sup>[6,7]</sup> It also offers large surface area with hydroxyl groups that can be functionalized through several different nanonization methods and classical chemical modifications.

Nanocomposites containing CNC can be processed via four different routes.<sup>[8–11]</sup> The first route is commonly known as solvent or solution casting, where initially, CNC is dispersed in a solvent first, in which the polymer matrix is also soluble then the nanocomposites are obtained by casting and drying (evaporation of solvent).<sup>[8,11–14]</sup> Second, route is based on in situ polymerization where CNC will be dispersed in the monomer or polymer precursors either with or without solvent and then it will be polymerized–cured.<sup>[15–17]</sup> In the third and *sol-gel* template method, percolating network of CNC is first formed by successive solvent exchange from the aqueous suspension of CNC and then the polymer–monomer is infused into this template.<sup>[18]</sup> This route is versatile and can achieve a high CNC loading and good dispersion of the CNC even in hydrophobic polymers.<sup>[19]</sup> In the fourth route, either CNC is melt-compounded with the host polymer matrix or first mixed with the monomer–precursors and then polymerized at softening or melting temperature of polymer through melt-compounding tools.<sup>[16,20,21]</sup> This route is highly preferred by polymer nanocomposites fabrication for the industrial-scale production, not only because it is viable through already existing infrastructure, it also offers multilayer coextrusion, melt-spinning of different polymers at a relatively more environmentally benign.<sup>[21–24]</sup> However, this approach for CNC incorporation has been so far limited by low thermal stability and the poor dispersion of acid-hydrolyzed CNC for reinforcing the majority of thermoplastics. Thermoplastic polyurethanes (TPU) are versatile polymers, have gained the utility across many application sectors owing to their attractive mechanical properties, including high tensile and tear strength, elongation, resilience, abrasion resistance, as well as their resistance to oils, grease, solvents, and chemicals.<sup>[25–30]</sup> In comparison to other nanoparticles, nanocellulose is an important reinforcing nanomaterial for reinforcing TPU, as it offers new appealing attributes from the aspect of sustainability, optical properties (transparency), and compliance. It also enables design of new functional materials<sup>[12,25,29,31–36]</sup> such as semi-interpenetrating network (IPN) polymer scaffolds,<sup>[37]</sup> strain sensors,<sup>[38,39]</sup> shape-memory biomedical materials,<sup>[31]</sup> self-healing coatings and healthcare materials,<sup>[40]</sup> and 4D

printable mechanically adaptive materials.<sup>[41]</sup> Generally, wet processing methods are commonly used in the academic reports on TPU nanocomposites with nanocellulose where organic solvents were involved with deplorable amounts, or industrially less favorable methods.<sup>[12,17,29,34,42–51]</sup> Surface-modified CNCs and thermally stable CNCs hydrolyzed from phosphoric acid have also been explored for melt extrusion.<sup>[22,52]</sup> We have previously reported solvent-free reactive extrusion (REX) of TPU nanocomposites using acid-hydrolyzed nanocellulose.<sup>[7]</sup> In our continued effort in cleaner (organic-solvent free) processing of polymer nanocomposites, we aimed to advance this methodology without the use of acid(s) or typical multiple-step acid-hydrolysis (including centrifuging, dialysis, ultrasonication, and freeze-drying). Herein, we report a more scalable and cleaner approach for TPU–CNC nanocomposites processing involving the following steps: (i) partial nanonization of microscale cellulose into CNC in deionized water using sonication, (ii) further in situ nanonization and CNC dispersion in polyol through scalable bead-milling, and then (iii) REX of the polyol–CNC dispersion with diisocyanate, and chain extender (Figure 1). In contrast to the acid-hydrolyzed long and thin nanocellulose,<sup>[7]</sup> nanocellulose in this study represents a most common low-aspect-ratio rod-like wood-based CNC. Hence, we have also compared and rationalized the structural changes and over-property profile enhancements.

## 2 | EXPERIMENTAL SECTION

### 2.1 | Materials

Microcrystalline cellulose (Avicel PH-101) (MCC) was used directly as obtained from FMC Biopolymer. 4,4'-diphenyl-methane diisocyanate (MDI), poly (tetramethylene glycol) (PTMEG) with a number average molecular weight ( $M_n$ ), 1000 g/mol, 1,4-butanediol (BDO), and dibutyltin dilaurate (DBTDL) was bought from Sigma-Aldrich and used as received.

### 2.2 | Preparation of polyol–CNC dispersions (through in situ nanonization)

The preparation of polyol–CNC dispersion involves three steps i) aqueous dispersion of MCC, ii) bead-milling of polyol–CNC dispersions, and iii) drying water from dispersions. The weighed amount of MCC was first mixed in deionized water (DI-H<sub>2</sub>O) by stirring at room temperature for 12 h (overnight) and then sonicated for 3 h in a bath sonicator (FXP12, LABEC) at an operating frequency of 40 kHz while replacing water every 60 minutes to control the heating. To this CNC dispersion, PTMEG

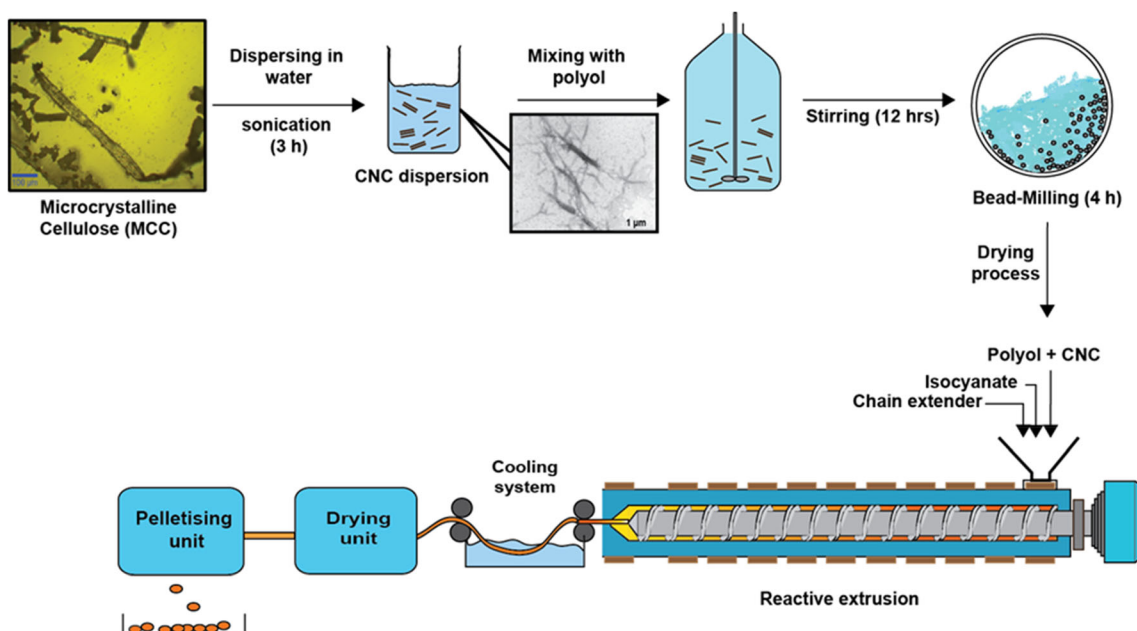


**FIGURE 1** Schematic representation of a scalable, acid-free in situ nanonization and organic solvent-free incorporation of CNC and processing of TPU-CNC nanocomposites via reactive extrusion

was added and allowed for stirring at room temperature for 12 h overnight. Subsequently, the suspension was homogenized for 1 min then transferred to the tank connected with an agitator bead mill (LabStar, Netzsch, Selb/Bavaria) with 0.4 mm zirconia beads for wet-milling. The milling with speed of 1500 rpm in continuous circulation mode was done at 40°C for 4 h. Then water was removed from the suspension by vacuum drying at 160°C using a thin wiped film evaporator (VTA, Germany) achieving a final water content in polyol-CNC below 300 ppm (as measured by Karl-Fischer moisture analysis). To avoid any further moisture absorption during handling and storage, dried nitrogen gas was purged into containers.

### 2.3 | Reactive extrusion process of TPU-CNC nanocomposites

Reactive extrusion of the polyol or polyol-CNC dispersions with BDO, MDI, and catalyst was performed according to the method described elsewhere.<sup>[53]</sup> In brief, TPU control and nanocomposites were processed in a 27 mm twin-screw extruder as illustrated in Figure S1 in Supporting Information (E-MAX Entek, Lebanon, [PA]), dropping the PTMEG 1000, MDI, and BDO at mass-flow rates of 1797.6 g/h (56.00 wt%), 254.8 g/h (36.06 wt%), and 1146 g/h (7.94 wt%), respectively, to achieve hard segment ratio 0.44, an NCO/OH stoichiometric ratio of 1:1 in order to obtain TPU with a shore hardness of 90A. The extrusion was performed at a screw speed of 90 rpm while maintaining the temperatures in barrel zones between

180 and 190°C. At output rate of 3.21 kg/h, the extrudate was obtained. For processing nanocomposites, the die temperature was increased to 180°C due to an increase in viscosity-torque. (Table S1 in Supporting information). Samples were denoted as “TPU-CNCA/B” in which A is CNC weight fraction and B is reaction stoichiometry. The sample films for characterization and properties measurements were obtained through compression-molding of the extrudates. In a pre-heated in-house designed hot-press machine, the samples were pressed between the assembly of brass plates, Teflon sheets, and 1 mm rectangular spacer at a temperature between 170 and 180°C at 7 kPa hydraulic pressure. Subsequently obtained films were annealed at a temperature of 80°C for 12 h under vacuum, before they were used for characterization and properties measurements. ASTM-d-638-M-3 was used as guideline to cut the samples-film for tensile and hysteresis tests.

### 2.4 | Characterization

The dimension and morphology of CNC were observed via transmission electron microscopy (TEM, JEOL 1011). CNC suspension was spotted on a copper-palladium grid and was stained with 2% of aqueous uranyl acetate (UA) after it was dried. Then the sample was analyzed at 100 kV. For polyol-CNC dispersion, a small amount of samples was placed onto cryopins and sited in the chuck of a Leica UCF6 ultracryomicrotome (Leica Microsystems, Wetzlar, Germany) chilled to -80°C. Then by using diatome diamond-trimming knife, a rectangular block was

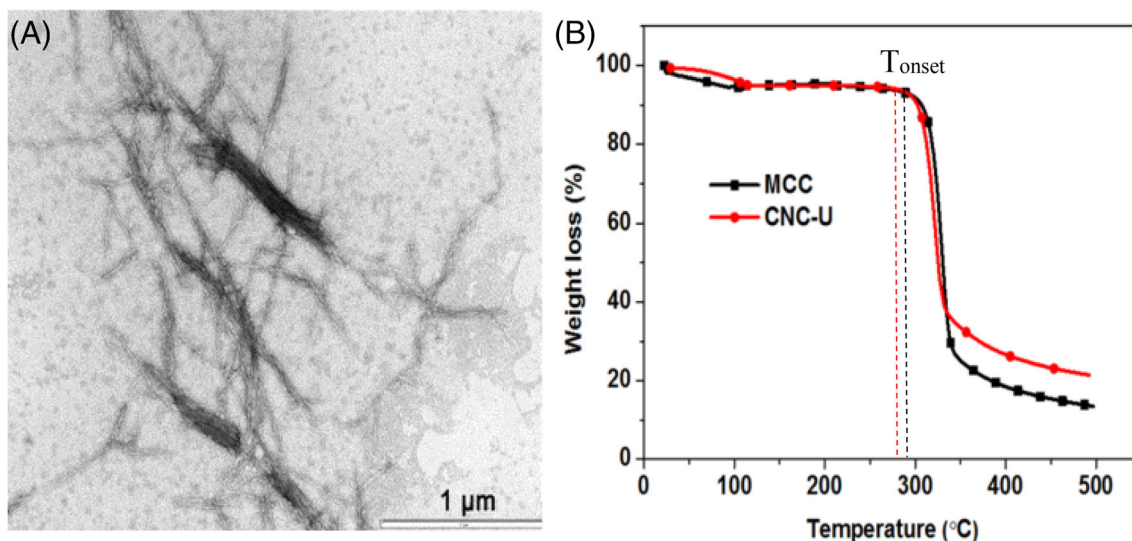


FIGURE 2 (A) TEM image and (B) TGA curve of CNC obtained from MCC after ultrasonication

cut from the sample. Approximately, 80–100 nm segments were cut using a cutting knife in the chamber with temperature of  $-100^{\circ}\text{C}$ . Then, the segments were put on formvar-coated copper palladium grids. After defrosting, the section was spotted with UA and incubated for 5–10 min. Subsequently, tip of paper was used to remove the UA; the sample was washed once with water and viewed under TEM once dried. The viscosity of polyol precursor was characterized using the controlled rheometer (AR-G2) with 20 mm parallel flat steel disk fixture. The test was conducted under isothermal condition at  $25^{\circ}\text{C}$  and at a shear rate sweep from  $0.1$  to  $100\text{ s}^{-1}$ .

Gel permeation chromatography (GPC) was used to determine the molecular weight of the extruded control TPU. The dilute solutions of TPU samples in tetrahydrofuran (THF) ( $1\text{ mg/ml}$ ) were analyzed a pre-calibrated GPC (Waters 1515) using narrow  $M_w$  polystyrene (PS) standards ( $M_w$ :  $1200$  to  $2 \times 10^6\text{ g/mol}$ , PDI:  $1.03$ – $1.06$ ) and the molecular weights ( $M_w$  and  $M_n$ ) were estimated with respect to PS standards using Empower Pro software. The molecular weight of TPU-CNC nanocomposite samples were not measured due to the possibility of CNC entering the separation column of GPC.

Infrared spectra were collected for all the samples using a Fourier transform infrared spectrometer (Nicolet 5700 spectrometer) equipped with a diamond attenuated total reflection (ATR) accessory, in a wavenumber range of  $525$  to  $4000\text{ cm}^{-1}$  averaged from 32 scans.

## 2.5 | Thermal and thermomechanical analysis

The thermal stability of CNC was analyzed under nitrogen atmosphere by thermogravimetric analysis (TGA)

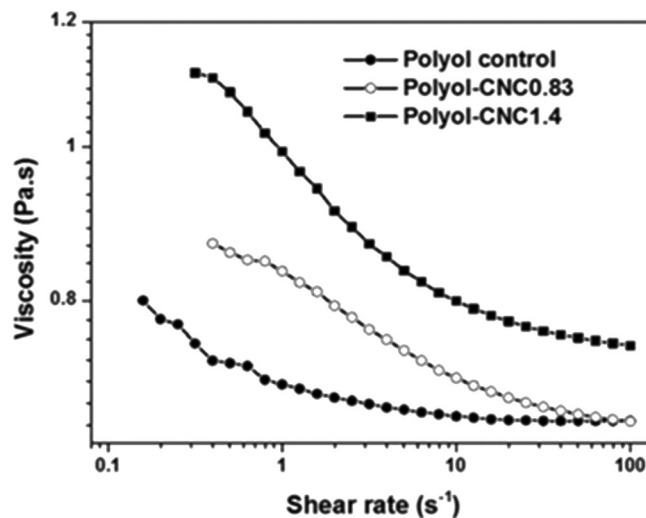


FIGURE 3 Viscosity as a function of shear rate of polyol control and polyol-CNC dispersions at 0.83 and 1.4 wt% CNC loading

using a “Mettler Toledo DSC/TGA Star<sup>e</sup>.” Initially, with a heating rate of  $10^{\circ}\text{C/min}$ , the samples were heated from  $27^{\circ}\text{C}$  to  $110^{\circ}\text{C}$  and were held for 10 min isothermally. Then it was heated to  $500^{\circ}\text{C}$  with rate of  $5^{\circ}\text{C/min}$ . A differential scanning calorimeter (Mettler Toledo DSC 1 Star) was used to analyze the thermal transitions of the TPU control and nanocomposites. The heating was programmed from  $-100^{\circ}\text{C}$  to  $300^{\circ}\text{C}$  at a rate of  $10^{\circ}\text{C/min}$  under a constant nitrogen flow. Thermomechanical properties consist of storage modulus ( $E'$ ) and  $\tan \delta$  ( $E''/E'$ ) were measured using Mettler Toledo instrument (SDTA861e) between a temperature range from  $-100$  to  $110^{\circ}\text{C}$  at a heating rate of  $3^{\circ}\text{C/min}$ , with frequency of  $2\text{ Hz}$  under tensile mode.

## 2.6 | Mechanical testing for TPU and TPU–CNC nanocomposites

Tensile properties of the samples were measured at room temperature using an Instron model 5543 universal testing machine equipped with a 500 N load cell with 14 mm and 50 mm/min of specimen gauge length and crosshead speed, respectively. Five and three replicates were done for tensile and hysteresis, respectively. The tear test was carried out according to the Method B of ISO 34-1 using angle-type (type B without a nick) specimen with crosshead speed of 500 mm/min. Creep behavior with 6 h duration according to the ISO 899-1, with stress hold at 2 MPa was performed using three replicates of sample. From the creep behavior curves, the creep resistance ( $E_t$ ) was estimated from these curves as the ratio of applied stress to tensile creep strain. Meanwhile, hysteresis test was performed under cyclic conditions of loading and unloading with stress up to different strain levels (50, 100, 200, and 500%). With the same specimen, each test was done for up to five cycles.

## 3 | RESULTS AND DISCUSSION

### 3.1 | CNC dispersion in polyol

MCC was dispersed in polyol by mechanical stirring, sonication, and then subsequently through bead-milling. Figure 2 displays the TEM micrograph and TGA graphs of CNC obtained via ultrasonication process. From Figure 2A, well-separated rod-like CNC can be predominantly seen with a width of about 30 nm and a length of approximately 500 nm. Nevertheless, partially deconstructed CNC, approximately with diameter of 70 nm and length 900 nm were also spotted signifying the tendency of CNC forming agglomeration due to strong secondary interactions like hydrogen bonding and van der Waals exist between CNCs. Meanwhile, thermal stability of the CNC was determined as well to ensure its processability at typical TPU processing temperatures. Figure 2B displays the onset degradation temperature ( $T_{\text{onset}}$ ) of CNC was recorded at 285°C yet it is slightly decreased from MCC ( $T_{\text{onset}} = 295^\circ\text{C}$ ). This difference is consistent with our earlier observation with mechanically deconstructed CNCs, attributed to the possible delamination of cellulose chains.<sup>[54]</sup> It also formed higher residual char than MCC powder, potentially due to enhanced deoxygenation reaction from the delaminated cellulose domains.

The milling of polyol/water/CNC could facilitate further nanonization and dispersion of CNC. During milling, the forces wielded between the colliding beads may

additionally fibrillate and break up the CNC agglomerate in polyol. The rheological properties of polyol and polyol–CNC dispersions tested after 4 h of bead-milling and subsequent vacuum drying, showed an increase in shear viscosity (Figure 3). It may indicate the enhancement in interactions between CNC and polyol via hydrogen bonding and van der Waals interactions. Since the dispersed CNC can perform as association surfaces for the crystallization of the polyol or as nucleation point, the polyol–CNC dispersions showed fiber-like aggregates in the electron microscopy images (Figure S2 in Supporting information) and a melting temperature  $\sim 20^\circ\text{C}$  with slight increase in the enthalpy of fusion from 79.9 to 83.2 Jg<sup>-1</sup> for polyol–CNC0.83 and 81.4 Jg<sup>-1</sup> for polyol–CNC1.4. (Figure S3 in Supporting information). The increase in viscosity had a significant influence on the processability of nanocomposites. Therefore, in practice, CNC with minimum amount volume had to be kept, or alternatively, lower viscosities polyols would have been chosen.

### 3.2 | Influence of in situ processed CNC on reactive extrusion of TPU

Compression molding of the extrudates resulted in a transparent film for both TPU control and TPU–CNC nanocomposites (Figure S4 in Supporting information). According to the gel permeation chromatography (GPC) analysis, TPU control obtained at an NCO/OH stoichiometric ratio of 0.99 had  $M_n$  of about 45,000 g/mol with PDI of 2.4. Meanwhile,  $M_n$  recorded a reduction to 49,000 g/mol and PDI to 2.3 when the stoichiometry was increased to 1, demonstrating the equimolar ratio of isocyanates and polyol. When the stoichiometric ratio was further increased to 1.01, significant increase in TPU molecular weight was recorded as  $M_n$  achieved 80,000 g/mol and PDI is 2.4. Above 1.01, white turbid semiliquid can be seen which represents the unreacted excess of isocyanate.

### 3.3 | Reinforcement effect of in situ processed CNC on TPU

#### 3.3.1 | Thermomechanical properties

The thermomechanical properties (storage modulus ( $E'$ ),  $\tan \delta$  ( $E''/E'$ )) measured using dynamic mechanical analysis (DMA) are shown in Figure 4. Both samples with and without CNC show changes in  $E'$  as typically found for multiphase elastomers upon temperature, that is, a high value (in the range of 2 to 3 GPa) in the glassy

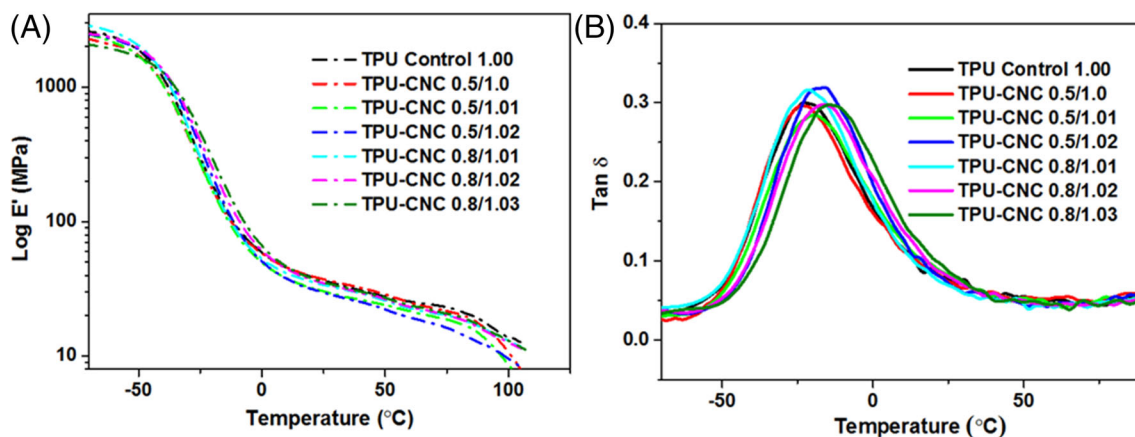


FIGURE 4 Thermomechanical properties (A) storage modulus and (B)  $\tan \delta$  of TPU control and TPU-CNC nanocomposites

TABLE 1 Influence of CNC content and stoichiometric ratios on the thermomechanical and tensile properties of TPU and TPU-CNC nanocomposites ( $\pm$  represents the SD of  $n = 5$ )

Materials	$E'$ at 25°C (MPa)	Damping peak (°C)	Tensile stress (MPa)	Tensile strain (%)	Young's modulus (MPa)	Toughness (MPa)	Tear strength (N/mm)	Creep modulus ( $E_c$ ) (MPa)
TPU control 1.00	37.7	-19.8	49.4 $\pm$ 1	1179 $\pm$ 28	16.0 $\pm$ 2	268.5 $\pm$ 10	113.5 $\pm$ 6	11.9
TPU-CNC0.5/1.0	29.1	-16.7	47.6 $\pm$ 2	1164 $\pm$ 40	20.6 $\pm$ 1	263.2 $\pm$ 15	126.1 $\pm$ 2	12.6
TPU-CNC0.5/1.01	33.8	-21.4	54.6 $\pm$ 1	1119 $\pm$ 23	18.8 $\pm$ 2	276.6 $\pm$ 8	127.2 $\pm$ 7	11.1
TPU-CNC0.5/1.02	35.0	-16.7	50.3 $\pm$ 4	915 $\pm$ 42	18.1 $\pm$ 1	207.7 $\pm$ 20	121.6 $\pm$ 2	10.7
TPU-CNC0.8/1.01	17.1	-19.5	57.0 $\pm$ 1	1031 $\pm$ 16	20.4 $\pm$ 1	262.5 $\pm$ 6	125.2 $\pm$ 6	10.7
TPU-CNC0.8/1.02	16.3	-20.2	63.6 $\pm$ 4	1008 $\pm$ 30	20.5 $\pm$ 0	271.2 $\pm$ 16	117.7 $\pm$ 7	12.7
TPU-CNC0.8/1.03	17.4	-20.1	61.0 $\pm$ 2	958 $\pm$ 15	18.3 $\pm$ 1	248.8 $\pm$ 10	120.5 $\pm$ 8	9.3

region ( $T < -50^\circ\text{C}$ ), a gradual decrease in  $E'$  (to 16–38 MPa) over transition regime ( $-50$  to  $25^\circ\text{C}$ ) with a broad damping, and then a low  $E'$  of the rubbery region ( $T > 25^\circ\text{C}$ ). The  $E'$  values for all the samples at room temperature are summarized in Table 1 where no significant increase in  $E'$  and/or no trend in  $E'$  were observed for nanocomposites upon the increase of CNC loading and stoichiometric ratio. In the rubbery region, the slope of the curve may signify the degree of hydrogen bonding remains significantly unaffected at this low loading of CNC.

From the broadness and height of the damping peaks, it can display the degree of order and the freedom of motion of the macromolecules in the soft domain.<sup>[55]</sup> A broad  $\tan \delta$  peak from  $-65$  to  $30^\circ\text{C}$  can be observed for the TPU control indicating primary relaxation of soft-segment domains at different length scales present in the multi-phasic system. Upon the cellulose incorporation at different NCO/OH stoichiometries, though the peak area and height remain closer to the TPU control, slight variations in glass transition temperature ( $T_g$ ) as a shift in damping peak was observed (Table 1). A slight

increase (for the samples TPU-CNC0.5/1.0 and TPU-CNC0.5/1.02) indicates the reduced relaxation, the segments in these nanocomposites as compared to TPU control.<sup>[56,57]</sup>

### 3.3.2 | Tensile properties

The reinforcement effect of in situ deconstructed CNC can be observed from the tensile properties, which included tear strength, creep behavior, and hysteresis as shown in Figure 5 and Table 1. In Figure 5A, the stress-strain curves in area of the low strain region (below 200%), shows no remarkable change in stress values but significant improvement in high-strain region for TPU-CNC nanocomposites. Student's  $t$ -test was performed between TPU control and nanocomposites and statically showed significant improvement of mechanical properties ( $p < .05$ ). In comparison with control, TPU-CNC nanocomposites with CNC loading at 0.5 and 0.8 wt% shows a small increase in young's modulus. Meanwhile, the strain for nanocomposites with 0.5 wt% of CNC

loading and up to 1.01 stoichiometric ratio is almost retained. At this loading level, the soft segments may still be able to conform and deform under applied stress.<sup>[46]</sup> The tensile strain was affected remarkably at higher stoichiometric ratio (1.02 for 0.5 wt% and 1.03 for 0.8 wt%). The influence of NCO/OH stoichiometry on the tensile properties can be seen in Figure 5B. In comparison to TPU control (1.00), a decrease in tensile strength for TPU–CNC 0.5/1.00 can be ascribed to the stoichiometric offset presumably owing to the relatively additional hydroxyl groups rendered by CNCs. With a slight increase in stoichiometric ratios, remarkable enhancement in tensile strength was observed without drastic decrease in the elongation, and it was up to certain NCO/OH ratios, for instance, 1.01 and 1.02 for CNC loading at 0.5 and 0.8 wt%, respectively. Out of all, a notable enhancement of 28% increase in tensile strength was achieved for sample TPU–CNC0.8/1.02 up to 63.6 MPa from 49.4 MPa for TPU control. The improvement of tensile strength was further supported by toughness and tear strength values where 10% of enhancement in toughness at low CNC loading (0.5 wt%) with a 1.02 NCO/OH stoichiometric ratio can be attributed to the retained tensile strain. However, any further increase in NCO/OH ratio or CNC loading affected the toughness adversely. In addition, the influence of CNC incorporation can also be seen as significant improvement in the tear strength due to the cohesive interactions (hydrogen bonding, van der Waals) between the host matrix and CNC.

### 3.3.3 | Creep resistance

The creep behavior of TPU control and nanocomposites measured under an applied stress of 2 MPa for 6 h can be seen in Figure 5C. Upon the 2 MPa applied stress, all the samples showed an initial tensile strain of 9 to 11% and then reaching 14 to 18% after 6 h of applied stress. The difference between the control TPU and nanocomposites can be regarded as insignificant as Student's *t*-test revealed  $p > .05$ . The tensile-creep modulus ( $E_t$ ), which represents the creep resistance was evaluated from these curves as the ratio of applied stress to tensile creep strain.  $E_t$  of TPU–CNC nanocomposites slightly increased with the CNC addition nonetheless decreased with increasing stoichiometric ratio. The higher in  $E_t$  indicates enhanced stress-transfer between the polymer matrix and CNC and resistance of nanocomposites to viscoelastic deformation over time. This can be attributed to the improved phase-mixing and interfacial adhesion between nanocrystal and polymer matrix at an optimum

NCO/OH ratio, which might cause local resistance for segmental movements of polymer chains and consequently decrease the deformation.<sup>[7,58]</sup> However, at an off-ratio, the microphase separation might be affected due to poor phase-mixing and causing slippage for creep behavior.<sup>[7,59]</sup>

### 3.3.4 | Hysteresis (resilience) behavior

Hysteresis behavior reflects the energy dissipation over time by the different phases and/or the incorporated fillers throughout the polymer matrix. For all samples (see Figure S5 in Supplementary information), the curves show stiffening upon initial loading and followed by a rollover response for subsequent loading and then hysteresis loops with residual strains upon unloading.

The area covered by loops represents the energy dissipated throughout the matrix, while the residual strain (%) after each cycle represents the plastic deformation. A stepwise increase in residual strain was observed with increasing number and strain of the cycles (Table S2 in Supporting information). This trend becomes more prevalent for the 200% and 500% strain cycles. The incorporation of CNC showed a slight increase in residual strain for the cycles stretched up to 100%, but this influence disappeared for the high strain cycles. The increase in residual strain due to plastic deformation can be ascribed to the orientation of hard segment domains (in TPU control) and the orientation of CNC (in nanocomposites) upon stretching.<sup>[47,60–62]</sup>

A similar trend was observed for hysteresis values determined from the area under the loading and unloading curves. The hysteresis values for the first cycles of each strain level were higher than that for the remaining cycles. This is attributed to the softening of the system upon cyclic stress namely called Mullins effect.<sup>[35]</sup> This stress-softening effect was reflected as decrease in hysteresis values in further cycles. Table 2 compares the hysteresis values determined from second and fifth cycles for both the TPU control and nanocomposites. The influence of CNC was observed as a slight increase in the hysteresis values even after five cycles can be determined. This is due to internal friction increase owing to the interfacial interactions between the CNC and TPU matrix indicating the enhanced energy dissipation.<sup>[35,63]</sup>

Overall, the analysis on mechanical reinforcement effect implies that in order to obtain appreciable improvement in tensile properties without affecting the characteristic viscoelastic behavior of TPU, the optimum NCO/OH ratios are 1.01 and 1.02 for with 0.5 and 0.8 wt % of in situ deconstructed CNC, respectively.

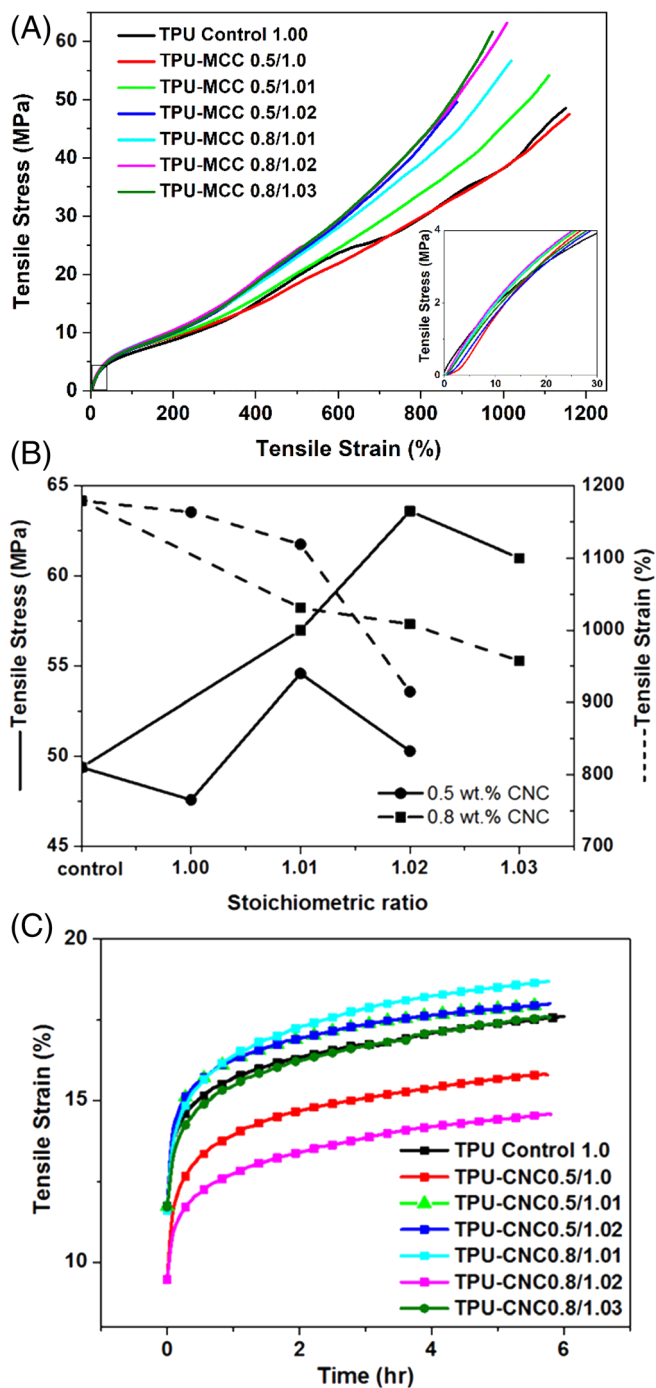


**FIGURE 5** (A) Tensile stress–strain curves of TPU and TPU–CNC nanocomposites (slope of the curve of low strain shows no significant changes [in the box]), (B) effect of stoichiometric ratio to tensile stress and strain, and (C) tensile-creep curves of the samples at an applied stress of 2 MPa for 6 h

### 3.4 | Structure-properties relationship

To understand the retained viscoelastic behavior (elongation, creep resistance, and hysteresis) while improving the strength of TPU, using in situ process with CNC, the samples were further characterized for

their chemical structural changes and thermal transitions.

Fourier Transform Infrared (FTIR) spectra revealed the influence of CNC loading and various NCO/OH ratio on chemical structural changes in TPU and nanocomposites. As the surface hydroxyl groups of CNC can be expected to interact with N–H and C=O functional groups of the growing polymer chains through hydrogen bonding, their association (Table 3) was quantitatively determined from the peak intensities of corresponding functional groups in FTIR spectra (Figure S6 in Supporting information). Their association behavior influences the physical properties of TPUs. For instance, the “free” N–H bonds (while being covalently connected with C=O groups to form urethane linkage render the elastic behavior, whereas the “associated” N–H is associated through hydrogen-bonding with C=O) enhances the association of hard-domains and secondary network formation.<sup>[51,64]</sup>

As shown in Table 3, a slight decrease in the associated “N–H” bonds upon with the addition of CNC and increasing NCO/OH ratio, indicate the reduction in association or hydrogen-bonding (ester–urethane and urethane–urethane) in hard and soft segment domains.<sup>[64,65]</sup> This was further reflected in the carbonyl groups as well (Figure S7 in Supporting Information). The carbonyl group association was examined in terms of degree of phase mixing (DPM) and/or separation (DPS), which represent carbonyl group associations via hydrogen bonding in hard segment–hard segment contact and/or that in hard segment–soft segment interactions.<sup>[66–68]</sup> Table 3 lists the R, DPS, and DPM values for TPU control and its nanocomposites. R is representing the carbonyl hydrogen bonding index. Lower DPM values were observed for TPU controls outside stoichiometry 1 (or  $1 \pm 0.01$  offset). Among the nanocomposites prepared, “TPU–CNC0.5/1.0,” whose stoichiometry is 1.0, has shown lowest DPM value. This may be due to the offset in stoichiometry attributed to the reaction between isocyanates and additional hydroxyl groups rendered by the CNC. Hence, further increase in the NCO/OH ratio in the CNC nanocomposites has shown DPM and DPS values closer to the TPU Control 1.0 and 1.01. In other words, “TPU–CNC0.5” nanocomposites with higher NCO/OH ratio than 1.0 have retained the same level of phase-separation of the TPU control. This observation is slightly different from our previous observation with thin, flexible, and high aspect ratio filament-like nanocellulose (diameter  $\sim 3\text{--}7$  nm) incorporated TPU nanocomposites, where the enhanced phase-mixing was observed.<sup>[7]</sup> Hence, in the current system upon the CNC addition and increasing NCO/OH ratio, physical nucleation of the hard segments (HS) on the rod-like low aspect ratio CNCs can be expected to occur predominantly rather than covalent linkage induced phase-mixing.



**TABLE 2** Hysteresis calculated on second and fifth loading–unloading cycle to 50, 100, 200, and 500%, respectively ( $\pm$  represents the SD value of  $n = 3$ )

Materials	Cycle	H <sub>50</sub> (MPa)	H <sub>100</sub> (MPa)	H <sub>200</sub> (MPa)	H <sub>500</sub> (MPa)
TPU control 1.0	2nd	0.33 ± 0	0.92 ± 0	2.74 ± 0	11.75 ± 0
	5th	0.25 ± 0	0.70 ± 0	1.96 ± 0	7.70 ± 0
TPU-CNC0.5/1.0	2nd	0.34 ± 0	0.93 ± 0	2.71 ± 0	11.33 ± 1
	5th	0.26 ± 0	0.71 ± 0	1.98 ± 0	7.45 ± 1
TPU-CNC0.5/1.01	2nd	0.32 ± 0	0.92 ± 0	2.84 ± 0	12.61 ± 0
	5th	0.25 ± 0	0.71 ± 0	2.06 ± 0	8.39 ± 0
TPU-CNC0.5/1.02	2nd	0.27 ± 0	0.85 ± 0	2.81 ± 0	13.74 ± 0
	5th	0.22 ± 0	0.66 ± 0	2.10 ± 0	9.43 ± 0
TPU-CNC0.8/1.01	2nd	0.27 ± 0	0.86 ± 0	2.91 ± 0	13.40 ± 0
	5th	0.21 ± 0	0.67 ± 0	2.12 ± 0	9.07 ± 0
TPU-CNC0.8/1.02	2nd	0.29 ± 0	0.84 ± 0	2.64 ± 0	11.86 ± 0
	5th	0.22 ± 0	0.65 ± 0	1.91 ± 0	7.92 ± 0
TPU-CNC0.8/1.03	2nd	0.28 ± 0	0.87 ± 0	2.80 ± 0	13.50 ± 0
	5th	0.23 ± 0	0.68 ± 0	2.09 ± 0	9.21 ± 0

**TABLE 3** Influence of CNC content and stoichiometric ratios on the degree of association, phase mixing, and phase segregation

Materials	Frequency shift ( $\Delta\nu$ ) (cm <sup>-1</sup> )	“Bonded N–H”	“Free” C=O (1729 cm <sup>-1</sup> )	Bonded C=O (1700 cm <sup>-1</sup> )	A <sub>1700</sub>	A <sub>1729</sub>	R	DPM	DPS
TPU control 0.99	129	16.2	18.6	4.0	0.69	0.39	1.77	36	64
TPU control 1.0	130	19.7	18.4	7.9	0.67	0.43	1.56	39	61
TPU control 1.01	131	17.2	19.5	7.7	0.70	0.41	1.71	37	63
TPU–CNC0.5/1.0	125	16.9	18.4	6.0	0.69	0.34	2.03	33	67
TPU–CNC0.5/1.01	126	17.7	19.2	7.8	0.69	0.41	1.68	37	63
TPU–CNC0.5/1.02	126	16.2	19.1	6.9	0.70	0.37	1.89	35	65
TPU–CNC0.8/1.01	130	17.1	19.5	8.0	0.69	0.43	1.60	38	62
TPU–CNC0.8/1.02	128	16.3	20.2	8.0	0.69	0.42	1.64	38	62
TPU–CNC0.8/1.03	130	17.4	20.1	8.2	0.69	0.44	1.57	39	61

This was further reflected in thermal transitions as characterized by DSC. In Figure 6, multiple endothermic transitions, which indicate the disruption and fusion of different phases and in different length scales in the multiphase TPU<sup>[26,69–71]</sup> can be observed for all the samples.

Table 4 summarizes the values of glass transition temperature ( $T_g$ ), multiple endothermic peaks (T1–T4), and the enthalpy for the fusion of the hard-segments, where **T1 in the range of 50–70°C indicates** the organizing of HS consist of single MDI, **T2 in the range of 100–180°C** reflects the glass transition of hard-segments and severance of numerous degrees of short-range HS comprised of MDI<sub>2</sub>BDO, MDI<sub>3</sub>BDO<sub>2</sub> blocks, **T3 in the range of 190–210°C shows the** higher melting of hard microphase, and **T4 in the range of 211–217°C represents** the disruption of predominantly MDI<sub>4</sub>BDO<sub>3</sub> and MDI<sub>5</sub>BDO<sub>4</sub> hard segment structures.

For the nanocomposites,  $T_g$  was slightly increased, which indicates restricted mobility of TPU chains at low temperatures attributing to the increased hard domains due to CNC-induced nucleation for crystallization. While *T1* and *T2* range, all the TPU–CNC nanocomposites displayed slight variations, whereas in *T3*-range, the nanocomposites with 0.8 wt% CNC at a higher stoichiometric ratio of 1.02 and 1.03 have shown endothermic peaks. This indicates that the formation of hard domain microphase due to the attachment of HS on the surface of CNC becomes distinct. *T4*-endothermic peaks, which are responsible for longer hard segment units in the chains, showed a slight increase for “TPU–CNC0.5/1.02” and “TPU–CNC0.8/1.02” with no clear trend upon CNC incorporation. The changes in *T3* and *T4* observed for nanocomposites can be presumably related to the morphological changes induced by the CNCs. With

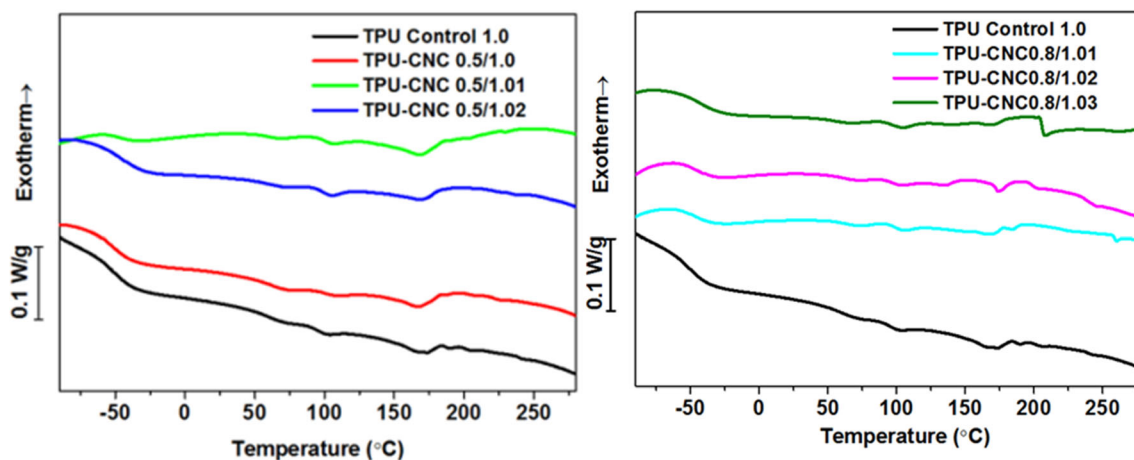


FIGURE 6 DSC thermograms of TPU control and TPU-CNC nanocomposites

Materials	$T_g$ (soft)(°C)	Endotherm peaks (°C)				Enthalpy $\Delta H^a$ (J/g)
		T1	T2	T3	T4	
TPU control 1.0	-55	69	102	190	242	3.35
			174	205		
TPU-CNC0.5/1.0	-48	72	108	-	225	6.01
			167			
TPU-CNC0.5/1.01	-48	68	106	-	-	7.25
			168			
TPU-CNC0.5/1.02	-44	-	137	-	260	3.88
			169			
TPU-CNC0.8/1.01	-49	68	105	-	-	2.59
			173			
TPU-CNC0.8/1.02	-43	70	103	203	245	4.55
			137			
TPU-CNC0.8/1.03	-46	68	105	208	-	3.12
			174			

TABLE 4 Thermal transitions and total enthalpy of fusion of TPU and TPU-CNC nanocomposites

<sup>a</sup>The sum of the  $T1$ - $T4$  melting enthalpies.

increasing MCC content in the polyol-water dispersion (aiming for 0.8 wt% CNC in final nanocomposites), the degree of nanonization and dispersion of CNC might be affected due to the viscosity increase.

Based on the degree of phase-mixing from FTIR analysis and the changes in  $T3$  and  $T4$  transitions from DSC, the morphological changes induced by the CNCs upon the NCO/OH increase are schematically represented in Figure 7 where rod-like shape (yellow) represent CNCs and the blue color represent hard segment formation (although the changes are relatively small, it not to be scaled). In TPU control 1.0, the hard domains (in Figure 7A) are formed through *hard*-HS interactions via hydrogen bonding and their microstructure and content depend on the

composition and DPM. In nanocomposites, depending on the dispersion, CNCs may act as nucleation points for the attachment of HS. In TPU, typically, the hard domains of 5–10 nm thick are formed, and the relatively larger CNC could be tethering between hard and soft segment domains.<sup>[46]</sup> Moreover, the nucleation points for crystallization (or hard-segment association) might increase upon the CNC incorporation and increase in NCO/OH ratio, as represented in Figure 7B. The additional HS formation in the nanocomposite systems was supported by a high  $T4$  transition observed for TPU-CNC0.5/1.02. Figure 7C illustrates the systems where hard-segment attachment increases with NCO/OH ratio along with possible bundles or agglomerates of CNCs are also present, for example,

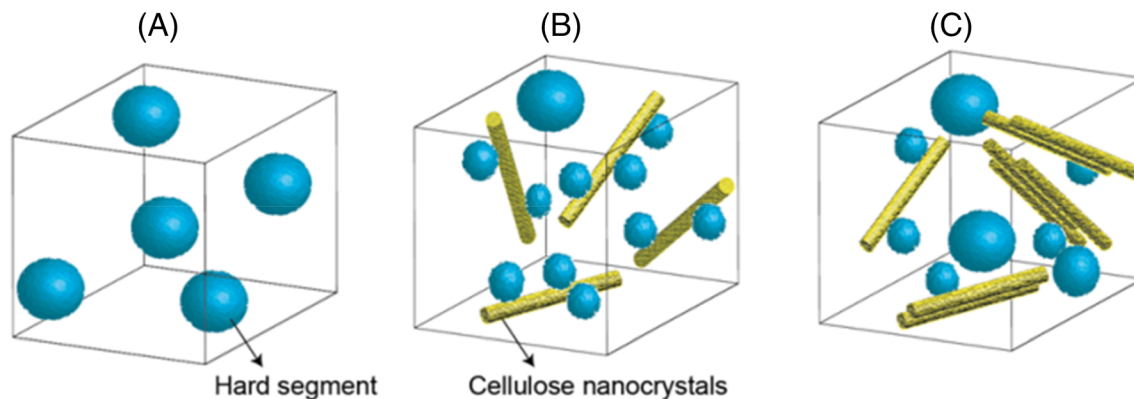


**FIGURE 7** Schematic representation of morphological changes induced by CNCs showing (A) hard-segment (blue sphere) in the TPU, (B) and (C) the attachment of hard-segment on the CNC surface. (B) Represents a well-dispersed system and (C) represents partially aggregated CNC containing system

TPU-CNC0.8/1.02 and TPU-CNC0.8/1.03. Furthermore, the heterogeneity in the dimension and dispersion of CNC may also affect the nucleation of HS. These morphological changes can explain the differences in the optimum levels of NCO/OH ratio for corresponding CNC loading levels, for improving tensile properties. For example, the decrease in elongation %, toughness, and tensile-creep modulus  $E_t$  values and increase in hysteresis values upon increase in NCO/OH ratio higher than optimum (1.01 for 0.5% and 1.02 for 0.8%) can be due to the low soft to hard segment ratio, the restricted mobility of chains in the hard domains formed by CNC induced nucleation (via hydrogen bonding) (Figure 7B) and possible bundles-agglomerations of low-aspect-ratio of CNCs (Figure 7C). This observation is contrary to our previous REX study with very high-aspect ratio nanocellulose<sup>[7]</sup> where the improvement in toughness was retained due to the enhanced phase-mixing and stepwise uncoiling and elongation of filament-like nanocellulose.

## 4 | CONCLUSIONS


In this study, we successfully demonstrated a cleaner and scalable approach for processing high performance (90A) TPU nanocomposites reinforced with CNC by the in situ deconstruction of cellulose microparticles in water and polyol through scalable mechanical methods and then reactive extrusion. The CNC prepared in this study exhibited higher-retained thermal stability for melt-processing as compared to CNC isolated via sulfuric acid-hydrolysis method. TPU-CNC nanocomposites prepared with a stoichiometric ratio of up to 1.01 for 0.5 wt% and 1.02 for 0.8 wt% CNC loading, displayed a remarkable improvement in tensile strength (up to 28%), toughness, and tear strength without significant compliance on inherent elastic properties of TPU

matrix. They have also exhibited modest improvement in creep resistance and resilience. Correlation between the FTIR spectral analysis and thermal transitions have also suggested the optimum NCO/OH ratio for reactive extrusion TPU with CNC. Hence, we conclude that this processing approach could be an attractive solution for processing polymer nanocomposites with a range of nanoparticles, which can be easily dispersed in water, incorporated into suitable precursors without any organic solvents, and processed via classical reactive extrusion processing methods.

## ACKNOWLEDGMENTS


Khairatun Najwa Mohd Amin gratefully acknowledges the Ministry of Higher Education Malaysia and Universiti Malaysia Pahang for the research fellowship for this study. Pratheep K. Annamalai acknowledges the Queensland Government for the Advance Queensland Research Fellowship (AQRf). The authors gratefully acknowledge the facilities as well as the scientific and technical assistance by the staff (Dr. Isabel C. Morrow) in the Australian Microscopy and Microanalysis Research Facility (AMMRF) at the Center for Microscopy and Microanalysis (CMM), the University of Queensland. Open access publishing facilitated by The University of Queensland, as part of the Wiley - The University of Queensland agreement via the Council of Australian University Librarians.

## ORCID

Khairatun Najwa Mohd Amin  <https://orcid.org/0000-0002-3221-2759>

Celine Chaleat  <https://orcid.org/0000-0002-0403-7236>

Grant Edwards  <https://orcid.org/0000-0001-7830-0204>

Darren J. Martin  <https://orcid.org/0000-0002-8537-6765>

Pratheep Kumar Annamalai  <https://orcid.org/0000-0002-7284-0813>

## REFERENCES

- [1] A. P. Kumar, D. Depan, N. Singh Tomer, R. P. Singh, *Prog. Polym. Sci.* **2009**, *34*, 479.
- [2] J. Jordan, K. I. Jacob, R. Tannenbaum, M. A. Sharaf, I. Jasiuk, *Mater. Sci. Eng., A* **2005**, *393*, 1.
- [3] K. Müller, E. Bugnicourt, M. Latorre, M. Jorda, Y. E. Sanz, J. M. Lagaron, O. Miesbauer, A. Bianchin, S. Hankin, U. Bözl, G. Pérez, M. Jesdinszki, M. Lindner, Z. Scheuerer, S. Castelló, M. Schmid, *Nanomater. (Basel, Switzerland)* **2017**, *7*, 74.
- [4] R. J. Moon, A. Martini, J. Nairn, J. Simonsen, J. Youngblood, *Chem. Soc. Rev.* **2011**, *40*, 3941.
- [5] S. Mondal, *Polym.-Plast. Technol. Eng.* **2018**, *57*, 1377.
- [6] S. J. Eichhorn, A. Dufresne, M. Aranguren, N. E. Marcovich, J. R. Capadona, S. J. Rowan, C. Weder, W. Thielemans, M. Roman, S. Rennecker, W. Gindl, S. Veigel, J. Keckes, H. Yano, K. Abe, M. Nogi, A. N. Nakagaito, A. Mangalam, J. Simonsen, A. S. Benight, A. Bismarck, L. A. Berglund, T. Peijs, *J. Mater. Sci.* **2010**, *45*, 1.
- [7] K. N. M. Amin, N. Amiralian, P. K. Annamalai, G. Edwards, C. Chaleat, D. J. Martin, *Chem. Eng. J.* **2016**, *302*, 406.
- [8] P. K. Annamalai, K. L. Dagnon, S. Monemian, E. J. Foster, S. J. Rowan, C. Weder, *ACS Appl. Mater. Interfaces* **2014**, *6*, 967.
- [9] J. Sapkota, S. Kumar, C. Weder, E. J. Foster, *Macromol. Mater. Eng.* **2015**, *300*, 562.
- [10] K. B. Azouz, E. C. Ramires, W. Van den Fonteyne, N. El Kissi, A. Dufresne, *ACS Macro Lett.* **2012**, *1*, 236.
- [11] K. Oksman, Y. Aitomäki, A. P. Mathew, G. Siqueira, Q. Zhou, S. Butylina, S. Tanpichai, X. Zhou, S. Hooshmand, *Compos. Part A Appl. Sci. Manuf.* **2016**, *83*, 2.
- [12] J. C. Natterodt, W. Meesorn, J. O. Zoppe, C. Weder, *Macromol. Mater. Eng.* **2018**, *303*, 1700661.
- [13] H. Pan, L. Song, L. Ma, Y. Hu, *Ind. Eng. Chem. Res.* **2012**, *51*, 16326.
- [14] Y. Wang, H. Tian, L. Zhang, *Carbohydr. Polym.* **2010**, *80*, 665.
- [15] X. M. Dong, T. Kimura, J.-F. Revol, D. G. Gray, *Langmuir* **1996**, *12*, 2076.
- [16] A.-L. Goffin, J.-M. Raquez, E. Duquesne, G. Siqueira, Y. Habibi, A. Dufresne, P. Dubois, *Biomacromolecules* **2011**, *12*, 2456.
- [17] W. Li, J. Yue, S. Liu, *Ultrason. Sonochem.* **2012**, *19*, 479.
- [18] J. R. Capadona, K. Shanmuganathan, D. J. Tyler, S. J. Rowan, C. Weder, *Science (80-. )* **2008**, *319*, 1370.
- [19] M. Jorfi, P. K. Annamalai, C. Weder, *Handb. GREEN Mater. 2 Bionanocomposites Process. Charact. Prop.*, World Scientific, Cambridge, UK **2014**, p. 23.
- [20] A. Junior de Menezes, G. Siqueira, A. A. S. Curvelo, A. Dufresne, *Polymer (Guildf)*. **2009**, *50*, 4552.
- [21] K. Oksman, A. P. Mathew, D. Bondeson, I. Kvien, *Compos. Sci. Technol.* **2006**, *66*, 2776.
- [22] A. Redondo, S. Chatterjee, P. Brodard, L. T. J. Korley, C. Weder, I. Gunkel, U. Steiner, *Polymers (Basel)*. **1912**, *2019*, 11.
- [23] K. M. Van de Voorde, J. K. Pokorski, L. T. J. Korley, *Macromolecules* **2020**, *53*, 5047.
- [24] B. Willocq, R. K. Bose, F. Khelifa, S. J. Garcia, P. Dubois, J.-M. Raquez, *J. Mater. Chem. A* **2016**, *4*, 4089.
- [25] J. J. Fallon, B. Q. Kolb, C. J. Herwig, E. J. Foster, M. J. Bortner, *J. Appl. Polym. Sci.* **2019**, *136*, 46992.
- [26] B. Finnigan, D. Martin, P. Halley, R. Truss, K. Campbell, *Polymer (Guildf)*. **2004**, *45*, 2249.
- [27] I. Rivera, D. Martin, R. Truss, *J. Polym. Eng.* **2006**, *26*, 903.
- [28] L. D. Tijing, M. T. G. Ruelo, A. Amarjargal, H. R. Pant, C.-H. Park, D. W. Kim, C. S. Kim, *Chem. Eng. J.* **2012**, *197*, 41.
- [29] S. Xu, D. Liu, Q. Zhang, Q. Fu, *Compos. Sci. Technol.* **2018**, *156*, 117.
- [30] D. Yuan, D. Pedrazzoli, G. Pircheraghi, I. Manas-Zloczower, *Polym.-Plast. Technol. Eng.* **2017**, *56*, 732.
- [31] I. T. Garces, S. Aslanzadeh, Y. Boluk, C. Ayranci, *J. Thermoplast. Compos. Mater.* **2020**, *33*, 377.
- [32] M. Lee, M. H. Heo, H.-H. Lee, Y.-W. Kim, J. Shin, *Carbohydr. Polym.* **2017**, *159*, 125.
- [33] A. Nicharat, A. Shirole, E. J. Foster, C. Weder, *J. Appl. Polym. Sci.* **2017**, *134*, 45033.
- [34] A. Pei, J.-M. Malho, J. Ruokolainen, Q. Zhou, L. A. Berglund, *Macromolecules* **2011**, *44*, 4422.
- [35] T. Sui, E. Salvati, S. Ying, G. Sun, I. P. Dolbnya, K. Dragnevski, C. Prisacariu, A. M. Korsunsky, *Sci. Rep.* **2017**, *7*, 916.
- [36] Y. Zhu, J. Hu, H. Luo, R. J. Young, L. Deng, S. Zhang, Y. Fan, G. Ye, *Soft Matter* **2012**, *8*, 2509.
- [37] M. Shahrousvand, M. Ghollasi, A. A. K. Zarchi, A. Salimi, *Int. J. Biol. Macromol.* **2019**, *138*, 262.
- [38] L. Zhu, X. Zhou, Y. Liu, Q. Fu, *ACS Appl. Mater. Interfaces* **2019**, *11*, 12968.
- [39] Q. Li, R. Yin, D. Zhang, H. Liu, X. Chen, Y. Zheng, Z. Guo, C. Liu, C. Shen, *J. Mater. Chem. A* **2020**, *8*, 21131.
- [40] H. Bi, Z. Ren, G. Ye, H. Sun, R. Guo, X. Jia, M. Xu, *Cellulose* **2020**, *27*, 8011.
- [41] T. W. Seguin, J. J. Fallon, A. Das, E. A. Holz, M. R. Bracco, J. E. Yon, E. J. Foster, M. J. Bortner, *Green Mater.* **2021**, *40*, 1.
- [42] K. Benhamou, H. Kaddami, A. Magnin, A. Dufresne, A. Ahmad, *Carbohydr. Polym.* **2015**, *122*, 202.
- [43] B. M. Cherian, A. L. Leão, S. F. de Souza, L. M. M. Costa, G. M. de Olyveira, M. Kottaisamy, E. R. Nagarajan, S. Thomas, *Carbohydr. Polym.* **2011**, *86*, 1790.
- [44] A. Dufresne, *Int. Polym. Process.* **2012**, *27*, 557.
- [45] J. Lamaming, R. Hashim, O. Sulaiman, C. P. Leh, T. Sugimoto, N. A. Nordin, *Carbohydr. Polym.* **2015**, *127*, 202.
- [46] J.-C. Liu, D. J. Martin, R. J. Moon, J. P. Youngblood, *J. Appl. Polym. Sci.* **2015**, *132*, n/a.
- [47] J. Mendez, P. K. Annamalai, S. J. Eichhorn, R. Rusli, S. J. Rowan, E. J. Foster, C. Weder, *Macromolecules* **2011**, *44*, 6827.
- [48] R. Prativiera, E. Pollet, R. E. S. Bretas, L. Avérous, A. A. Lucas, *J. Appl. Polym. Sci.* **2018**, *135*, 46736.
- [49] L. Rueda, B. Fernández d'Arlas, Q. Zhou, L. A. Berglund, M. A. Corcuera, I. Mondragon, A. Eceiza, *Compos. Sci. Technol.* **2011**, *71*, 1953.
- [50] L. Rueda, A. Saralegi, B. Fernández-d'Arlas, Q. Zhou, A. Alonso-Varona, L. A. Berglund, I. Mondragon, M. A. Corcuera, A. Eceiza, *Cellulose* **2013**, *20*, 1819.
- [51] M. Ö. Seydibeyoğlu, K. Oksman, *Compos. Sci. Technol.* **2008**, *68*, 908.
- [52] R. Prativiera, E. Pollet, R. E. S. Bretas, L. Avérous, A. de Almeida Lucas, *J. Appl. Polym. Sci.* **2021**, *138*, 50343.
- [53] K. N. Mohd Amin, *Ph.D Thesis*, Australian Institute for Bio-engineering and Nanotechnology, The University of Queensland, Australia **2016**. <https://doi.org/10.14264/uql.2016.562>.
- [54] K. N. M. Amin, P. K. Annamalai, I. C. Morrow, D. Martin, *RSC Adv.* **2015**, *5*, 57133.
- [55] T. W. Son, D. W. Lee, S. K. Lim, *Polym. J.* **1999**, *31*, 563.

- [56] M. L. Auad, M. A. Mosiewicki, T. Richardson, M. I. Aranguren, N. E. Marcovich, *J. Appl. Polym. Sci.* **2010**, *115*, 1215.
- [57] A. Frick, A. Rochman, *Polym. Test.* **2004**, *23*, 413.
- [58] A. Boubakri, N. Haddar, K. Elleuch, Y. Bienvenu, *C. R. Méc.* **2011**, *339*, 666.
- [59] H. J. Qi, M. C. Boyce, *Mech. Mater.* **2005**, *37*, 817.
- [60] G. Ayoub, F. Zaïri, M. Naït-Abdelaziz, J. M. Gloaguen, G. Kridli, *Int. J. Plast.* **2014**, *54*, 19.
- [61] E. M. Christenson, J. M. Anderson, A. Hiltner, E. Baer, *Polymer (Guildf)*. **2005**, *46*, 11744.
- [62] B. R. Crenshaw, C. Weder, *Macromolecules* **2006**, *39*, 9581.
- [63] H. Xia, S. J. Shaw, M. Song, *Polym. Int.* **2005**, *54*, 1392.
- [64] C. M. Brunette, S. L. Hsu, W. J. MacKnight, *Macromolecules* **1982**, *15*, 71.
- [65] C. Zhang, J. Hu, S. Chen, F. Ji, *J. Mol. Model.* **2010**, *16*, 1391.
- [66] C. W. Meuse, X. Yang, D. Yang, S. L. Hsu, *Macromolecules* **1992**, *25*, 925.
- [67] R. W. Seymour, G. M. Estes, S. L. Cooper, *Macromolecules* **1970**, *3*, 579.
- [68] Y. I. Tien, K. H. Wei, *Polymer (Guildf)*. **2001**, *42*, 3213.
- [69] D. J. Martin, G. F. Meijs, P. A. Gunatillake, S. J. McCarthy, G. M. Renwick, *J. Appl. Polym. Sci.* **1997**, *64*, 803.
- [70] S. Pongkitwitoon, R. Hernández, J. Weksler, A. Padsalgikar, T. Choi, J. Runt, *Polymer (Guildf)*. **2009**, *50*, 6305.
- [71] R. W. Seymour, S. L. Cooper, *Macromolecules* **1973**, *6*, 48.

### SUPPORTING INFORMATION

Additional supporting information may be found in the online version of the article at the publisher's website.

**How to cite this article:** K. N. Mohd Amin, C. Chaleat, G. Edwards, D. J. Martin, P. K. Annamalai, *Polym. Eng. Sci.* **2022**, *1*. <https://doi.org/10.1002/pen.25899>